OPTIMIZATION STRATEGIES FOR THE INTEGRATION OF LIDAR-DERIVED MULTI/HYPERSPECTRAL IMAGERY TO ENHANCE WETLAND CLASSIFICATION IN GREAT LAKES COASTAL WETLANDS

Zach Raymer

Journal article submitted in partial fulfillment of
the requirements for the degree of
Master of Science

Department of Geography

Central Michigan University
Mount Pleasant, Michigan
January 2012

Accepted by the Faculty of the College of Graduate Studies,

Central Michigan University, in partial fulfillment of

the requirements for the master's degree

Journal Article Committee:

Brian L. Becker, Ph.D.	Committee Chair
Bin Li, Ph.D.	Faculty Member
David K. Patton, Ph.D.	Faculty Member
March 2, 2012	Date of Defense
Roger Coles, Ed.D.	Dean College of Graduate Studies
March 26, 2012	Approved by the College of Graduate Studies

ACKNOWLEDGEMENTS

I would like to thank the members of my thesis committee, Dr. Bin Li and Dr. Dave Patton. Each has helped me throughout this research project, from formulating my research question, to reviewing the drafts of my article; they have provided invaluable insight as well as constantly pushing me to be a better writer. I would also like to thank the Michigan Space Grant Consortium for partial funding of this project. Finally, I would like to give my thesis advisor, Dr. Brian Becker a special thank you. He has always challenged me to improve myself both personally and academically, and without him, much of this research would not have been possible.

ABSTRACT

OPTIMIZATION STRATEGIES FOR THE INTEGRATION OF LIDAR-DERIVED MULTI/HYPERSPECTRAL IMAGERY TO ENHANCE WETLAND CLASSIFICATION IN GREAT LAKES COASTAL WETLANDS.

by Zach Raymer

The ability to remotely monitor Great Lakes Coastal Wetlands is important because it allows us to study a constantly changing ecosystem without spending hours in the field. However, identifying plant species commonly found in Great Lakes Coastal Wetlands from an airborne or spaceborne remote sensing platform can be a challenge due to the spectral similarities between many wetland plant species. The introduction of lidar, a laser based elevation mapping system, to the field of remote sensing has added an additional component that may be helpful in differentiating wetland plants. Using lidar data to approximate plant canopy height, we hope to determine the superior integration method for fusing lidar to spectral imagery. Two sets of imagery will be tested for superior integration methods, the first a 32 band hyperspectral image, and the second a synthetically derived aerial photography based on the 2009 NAIP bandset. Two classification routines, Maximum Likelihood and Neural Network, will be used to determine overall and cover type specific classification accuracies when testing superior lidar integration methods for each set of imagery. As hyperspectral sensors can be programmed to record spectral information for specific band combinations, an investigation was performed of the reduction of image spectral dimensionality after being fused with lidar data to determine at what spectral resolution overall or cover type specific classification accuracies begin to significantly decrease. The final focus of this paper was to determine how the addition of lidar data, specifically plant

canopy height, to a synthetically derived aerial photograph affected overall and cover type specific classification accuracies in comparison to a traditional hyperspectral image.

TABLE OF CONTENTS

LIST OF TABLES

TABLE PAGE

LIST OF FIGURES

FIGURE PAGE

CHAPTER I

INTRODUCTION

Background

Classifying wetland plant species is challenging due to the botanical similarities of many wetland plant species. This botanical 'closeness', relative to remote sensing, means many plant species commonly found in wetlands are spectrally very similar. Theoretically, each plant has a unique spectral signature which, in a laboratory setting, is uniquely identifiable (Reed, et al., 1994; Key, Warner, McGraw, & Fajvan, 2001). However, when trying to differentiate wetland plant species from an airborne or spaceborne remote sensing platform, the plants become less distinguishable spectrally.

Two primary components that contribute to the overall quality of an image are its spatial and spectral resolutions. Spatial resolution refers to sensor or image pixel size. The higher the spatial resolution of a sensor/image, the smaller of a geographic area a pixel represents; the lower the spatial resolution, the larger geographic area a pixel represents. The same is true for spectral resolution; images with high spectral resolution have an increased number of bands, each typically with a narrower bandwidth, while images with low spectral resolution have fewer bands, typically with broader bandwidths. While an increase in technological capabilities of remote sensing systems has led to a reduction in imagery costs, there is still a difference in price between low spatial/spectral resolution imagery (e.g. CIR aerial photography) and high spatial/spectral resolution imagery (e.g. hyperspectral imagery). This poses an important question in the field of remote sensing, "What data is ideal for any given application?" Anderson says a major advantage of hyperspectral remote sensing when differentiating plant communities at the species level is the exactness of the spectral response (Anderson, et al.,

2008). However, it is still unclear if the same results can be obtained using a dataset with a fewer bands. Some studies focused on reducing the spectral dimensionality of an image to include only the most meaningful spectral bands (Haskett & Sood, 1998; Plourde, Ollinger, Smith, & Martin, 2007; Underwood, Ustin, & Dipietro, 2003; Williams & Hunt Jr., 2002; Becker, Lusch, & Qi, 2005; Becker, Lusch, & Qi, 2007). By determining whether a spectrally reduced dataset, like digital infrared aerial photography, can achieve the same accuracies as a hyperspectral image, researchers can target their sensors to collect only the most relevant information. This can then help reduce overall acquisition cost and end-user image processing time via a strategically targeted imaging campaign.

Problem

The introduction of lidar in recent years has added an additional component to the field of wetland remote sensing. Lidar technology utilizes millions of discrete laser pulses (i.e. there are approximately 1 million laser pulses per square kilometer when 1m post spacing is used) to generate elevation data across a landscape. When a landscape is covered with vegetation, part of the return pulse measures surface elevation(s) of the plant canopy (i.e. first return) and part of the return measures the elevation of the actual ground surface (i.e. ground return). Thus, lidar data contains information related to the biophysical nature (e.g. plant height, surface texture, etc.) of the plant canopy, as well as elevation characteristics of the earth's surface. The existence of lidar data makes it possible to integrate this biophysical/elevation component with the spectral component to potentially increase the utility of remotely-sensed imagery. However, whether a lidar component adds significantly to the utility of an image remains in question. To date, the majority of research involving lidar has been focused on two categories; the first has investigated

methods for classifying lidar point clouds into ground and non-ground returns (Kraus & Pfeifer, 1998; Vosselman, 2000; Zhang, et al., 2003) and the second has centered on the classification of shape features like buildings and trees (Axelsson, 1999; Maas, 1999).

Numerous studies have shown that there is a complementary relationship between lidar and hyperspectral data because of the different information each dataset contains (Brennan & Webster, 2006; Hyde, Ross, Kimes, & Levine, 2007; Simental, Ragsdale, Bosch, Dodge, & Pazak, 2003; Mundt, Streutker, & Glenn, 2006). Lidar data provides a detailed record about ground as well as canopy elevations but lacks spectral information, whereas hyperspectral data provides a comprehensive spectral profile, but lacks elevation information (Dalponte, Bruzzone, & Gianelle, 2008). While lidar is a relatively new technology, there have been several studies that have shown the addition of lidar data to a classification routine can help improve the classification accuracy of a spectral dataset, at any spectral resolution (Anderson, et al., 2008; Gilmore, et al., 2008; Onojeghuo & Blackburn, 2011). Current hyperspectral imaging sensors are capable of capturing many narrow spectral bands from the visible domain to the near infrared region of the electromagnetic spectrum. This allows researchers to study features/land covers that are obscured in sensors with a lower spectral resolution (Govender, Chetty, Naiken, & Bulcock, 2008). Imagery with very high spectral resolution (i.e. hyperspectral imagery), has been shown to improve vegetation classification accuracy when compared to lower spectral resolution images (Yamano, Chen, & Tamura, 2003; Underwood, Ustin, & Dipietro, 2003; Galvao, Formaggio, & Tisot, 2005).

Lidar data can be used with the hyperspectral data to help separate plant species into their correct classes. For example, if there are two plant species, Plant A and Plant B, both of which have very similar spectral reflectance curves, but have different height characteristics, the

addition of lidar data would help to separate their classes in a classification routine, where hyperspectral alone could not. One such study has shown that using canopy height models (CHM), derived from subtracting a first return surface height model (DSM) and a ground return model (DEM), and slope derived from a DEM is an effective way to further refine classification results post-spectral classification (Onojeghuo & Blackburn, 2011). However it should be noted that Onojeghuo's study found CHM and slope to have negative effects on classification accuracies when used with spectrally compressed image data like PCA or MNF, whereas our study will not be using spectrally compressed data. As indicated in previous research (Bork & Su, 2007; Gilmore, et al., 2008; Jones, Coops, & Sharma, 2010), this study will demonstrate the advantages of using lidar in conjunction with hyperspectral imagery when classifying Great Lakes Coastal Wetlands (GLCWs) by combining hyperspectral data with the lidar-derived biophysical height properties of wetland plant communities.

Purpose

As technology has advanced, the capabilities of digital remote sensing systems have increased, both spatially and spectrally. This has led to a dramatic increase in the quality and quantity of data that can be collected from a sensor. One would expect this would lead to more accurate and resilient classification schemes, especially in botanically diverse areas like Great Lakes Coastal Wetlands. However it is unclear if this additional spatial and/or spectral information actually benefit researching concerning GLCWs. This study explored how combing spectral imagery data (both hyperspectral and 'synthetically derived aerial photography') with biophysical height properties derived from a lidar dataset will affect overall and cover type specific classification accuracies.

The benefits of researching this topic include determining the effects spectral dimensionality has on accuracy, as well as how these two relatively new technologies, which are increasingly being collected simultaneously, can be used together to create a more robust dataset. While there has been much research in the usefulness and applications of lidar to image classification problems (Bork & Su, 2007; Brennan & Webster, 2006; Dalponte, Bruzzone, & Gianelle, 2008), few have explored the fusion of biophysical measurements, specifically plant height, derived from lidar data, with spectral reflectance data. Some research has concentrated on fusing lidar with either multi or hyperspectral imagery to improve classification results (Gilmore, et al., 2008; Jones, Coops, & Sharma, 2010; Mundt, Streutker, & Glenn, 2006), while Onojeghuo & Blackburn (2011) concentrated on using lidar to improve classifications generated from hyperspectral imagery. Since lidar is a relatively new remote sensing tool, it is important to determine how it can benefit the remote sensing community, in addition to establishing its technological and practical shortcomings. By integrating the biophysical characteristics of wetland plants expressed through lidar data into multi and hyperspectral imagery, and then assessing how this additional information affects image classification accuracy, we can determine whether future research on wetland plant classification should incorporate lidar data in a classification routine.

Study Area

Wildfowl Bay island complex is located beside the southeastern shore of the Saginaw Bay in Lake Huron. Horseshoe Bay is a shallow embayment, protected by the Wildfowl Bay island complex. The island complex consists of three islands, Maisou, Middle Grounds, and Heisterman Island. The study site chosen for this analysis is a rectangle, covering the southeast

portion of the Wildfowl Bay island complex, including Horseshoe Bay in the northwest corner and ending with part of the mainland in the southeast corner of the study site. The wetland plants in the Wildfowl Bay island complex experience changes in abundance and distribution of vegetation types (Koonce, Minns, & Morrison, 1998) due to dramatic water-level fluctuations as a result of the shallow nature of the embayment wetlands in Saginaw Bay (Maynard & Wilcox, 1997). The emergent zones of the mainland are dominated by *Typha angustifolia* and *Phragmites australis*, however small colonies of less prevalent emergent genera (i.e. *Sagittaria, Pontenderia*) can also be found. The emergent zone within the bay proper is dominated by *Scirpus validus, Sagittaria rigida,* and *Typha angustifolia;* while the upper elevations of the island are dominated by facultative woody species and upland/wetland graminoids (Becker, 2002). This wetland region was chosen due to data availability and because the heterogeneous nature of the plant species found in the area offers a particularly suitable study site from a remote sensing standpoint. The size and location of the wetland makes it a prime example of the usefulness of remote sensing technologies. Through aerial imagery we have the opportunity to study a wetland plant community that would otherwise be relatively inaccessible to wetland researchers.

Figure 1. Horseshoe Bay Image Boundary and Surrounding Areas

CHAPTER II

RESEARCH OBJECTIVES

Research Objective One

The first objective of this research was to determine the ideal stretching method when integrating lidar data into imagery using two classification routines. Two sets of tests were performed. The first test compared stretching methods for the integration of lidar into hyperspectral imagery using both classification routines; the second test compared stretching methods for integrating lidar into synthetically derived aerial photography using both classification routines. To determine which stretching method produced the best results, the overall and cover type specific classification accuracies of the lidar fused imagery, for each stretching and classification method, were compared with the accuracies of the classification for both synthetic derived aerial photography and hyperspectral imagery.

Research Objective Two

The second objective of this research was to determine whether the integration of lidar data allows for a reduced spectral resolution (i.e. fewer spectral bands) without affecting overall and cover type specific classification accuracies. The number of bands in a hyperspectral image fused with ideally stretched lidar was systematically reduced based on the greatest spectral distance from the seven ideal bands identified by Becker, Lusch, & Qi (2005). After each subsequent band was removed, overall and cover type classification accuracies using two classification routines were compared to those classification accuracies achieved by the original hyperspectral imagery. This process was repeated until only two bands remained, as two bands is the minimum required to perform a classification.

Research Objective Three

The final objective of this research was to determine if a synthetically derived aerial photograph fused with ideally stretched lidar can achieve comparable overall and cover type classification accuracies using neural two classification routines to those classification accuracies achieved by original hyperspectral imagery.

CHAPTER III

METHODOLOGY

Data Collection

Hyperspectral Imagery

Both the hyperspectral and lidar imagery were collected on the same day in September 2010. The hyperspectral imagery was collected by a CASI-1500 spectrometer with a spatial resolution of 50cm and wavelength domain ranging from 374.5 -1040.9 nm separated into 32 bands, each with a bandwidth of approximately 20.8 nm. The hyperspectral imagery was radiometrically calibrated in ENVI using in-situ calibration coefficients collected during image capture. Subsets of the calibrated imagery were extracted to reduce the scope of the imagery to just the study site.

Synthetically Derived Aerial Photograph

To compare the classification accuracy of a spectrally reduced image fused with lidar to the baseline hyperspectral image, a 'synthetically derived aerial photograph' (SDAP) was created. This image was based on the bandset associated with the 2009 NAIP CIR aerial photography; the image will consist of four very wide reflectance bands, blue (400-580 nm), green (500-650 nm), red (590-675 nm), and near infrared (675-850 nm). To create this image, the original hyperspectral image was spectrally resampled to match the FWHM of each band in the NAIP imagery. The bands were layered to create the synthetically derived aerial photograph.

Lidar Data

From the lidar dataset, three raster elevation models were created, with each model being co-registered to both the hyperspectral imagery and the SDAP. The first model, a digital surface

model (DSM), was derived using only first return lidar points and represents the elevations of the top of the plant canopies. The second model, a bare-earth digital elevation model (DEM), was created using only ground return points and represents the elevation of the earth's surface without plant coverage. Finally the DEM was subtracted from the DSM to create a vegetation height model (VHM). The baseline VHM was then stretched using different stretching methods and fused to both the hyperspectral imagery and the synthetically derived aerial photography.

Ground Truth Data

Field or ground-truth data was collected on September 10 and 17, 2010. Using GPS, point, line and polygon botanical data was collected in select areas of the wetland complex via access by airboat. The edges of target plant communities were recorded (i.e. line data), points located in the center of homogeneous areas of a specific vegetation type (i.e. point data), and polygons that encapsulate homogenous regions of the dominant plant species present. After differential correction to increase spatial accuracy, the GPS data was used to generate cover type regions of interest (ROI's) in ENVI. Each cover type was separated into training and test ROI's. The training ROI's (Table 1) provide the statistical information for both of the supervised classification routines, while test ROI's (Table 2) were used to verify the accuracy of each classification. Due to variations in the spatial diversity or extent of the various botanical classes shown in Table 1 and 2, the relative size of each training/test ROI varied.

Table 1. Training class pixels (ENVI Regions of Interest)

ROI	Cover type	# of pixels
1	Wild Rice (*Zizania palustris)*	190
2	Cattails (*Typha latifolia)*	5,347
3	Phragmities (*Phragmities australis)*	4,255
4	Pickerelweed (*Pontederia cordata)*	555
5	Bulrush (*Scirpus acutus, Scirpus validus)*	542
6	Broad Leaf Arrowhead (*Sagittaria latifolia, Sagittaria rigida)*	80
7	Submergent Vegetation (*Vallisneria americana, Chara sp.*)	8,799
8	Open Water	11,560
9	Wet Meadow	1,911
10	Shrubs	195
11	Tree	1,096
12	SpikeRush (*Eleocharis sp.)*	355
13	Willows	473

Table 2. Test class pixels (ENVI Regions of Interest)

ROI	Cover type	# of pixels
1	Wild Rice (*Zizania palustris)*	192
2	Cattails (*Typha latifolia)*	5,179
3	Phragmities (*Phragmities australis)*	6,992
4	Pickerelweed (*Pontederia cordata)*	565
5	Bulrush (*Scirpus acutus, Scirpus validus)*	543
6	Broad Leaf Arrowhead (*Sagittaria latifolia, Sagittaria rigida)*	1,879
7	Submergent Vegetation (*Vallisneria americana, Chara sp.*)	10,443
8	Open Water	11,560
9	Wet Meadow	2,848
10	Shrubs	436
11	Tree	2,073
12	SpikeRush (*Eleocharis sp.)*	1,356
13	Willows	852

Data Processing

Classification Algorithms

Two classification algorithms, Maximum Likelihood (ML) and Neural Network (NN) were used in this study. The first algorithm, Maximum Likelihoood, is a commonly used

probability based classifier, and assumes the statistics of each training class are normally distributed for all participating bands. The ML classifier calculates the probability that a pixel belongs to a given class based on a preset probability threshold; each pixel is assigned to the class for which it has the highest probability of belonging, unless the probability threshold is not met, in which case the pixel remains unclassified. A probability threshold of .95 or approximately two standard deviations from the mean was chosen for this study. Maximum Likelihood was chosen as one of the classification routines because it has been shown in multiple studies to outperform other parametric classifiers (Shafri, Suhaili, & Mansor, 2007; Govender, Chetty, Naiken, & Bulcock, 2008; Kumar & Ramachandra, 2008). The second algorithm, Neural Network, is a feed-forward, non-linear classification routine that uses back-propagation for learning of training data. This classification method was chosen in part because it has been shown to produce higher accuracy classification results than algorithms using traditional statistical methods, and also because it makes no assumptions on the statistical distribution of the training data (Atkinson & Tatnall, 1997).

Stretching Methods

Five methods of stretching the VHM band were explored in this study. The first stretching method that was explored is 'no-stretch'. This simply means the VHM band contained original height values (i.e. meters) for each pixel when integrated into the hyperspectral image. The second method, linear stretching, stretched the input data between the preset minimum and maximum (the minimum and maximum reflectance values from the hyperspectral image) in a linear fashion. The third method, histogram equalized, stretched the data between the preset minimum and maximum while assigning an equal number of input DNs to each output histogram

bin. The fourth method, a Gaussian stretch, stretched the input data that fell within ± 3 standard deviations of the mean into a Gaussian distribution. The final stretching method, square root, took the square root of the input histogram and applied a linear stretch, fitting the output data to the preset minimum and maximum.

Data Analysis

The first research objective, determining the superior stretching method when integrating lidar data into imagery, was tested using two sets of classifications, one for the maximum likelihood classifier and one for the neural network classifier. First, the original (non-lidar) hyperspectral image was classified using neural network and maximum likelihood classification routines, and confusion matrices were generated for each method, comparing the overall accuracy, the average producers accuracy, and the cover type specific producer's accuracy (i.e. producer's accuracy is a measure of how many pixels of the test class were correctly classified.). The confusion matrices provided the classification accuracy standard, both overall and cover type specific, for which the accuracy of all test classifications was compared. Then the unstretched lidar-fused hyperspectral imagery was similarly classified using identical training class data. This process was repeated for all five stretch types to determine the ideal stretching method for both classification routines. Then the same classification and comparison process was repeated, using an original (non-lidar) synthetically derived aerial photograph as the basis for classification accuracy comparison, and lidar-fused synthetically derived aerial photography as the test classifications. The purpose of this was to determine whether the ideal stretch method for the VHM band changed for an image with lower spectral resolution.

To test the second objective, an original (non-lidar) hyperspectral image was classified using both the neural network and the maximum likelihood classification routines and were used as the basis of comparison for lidar-fused spectrally reduced imagery. Previous research suggests there needs to be a minimum of seven spectral bands, optimally placed, to achieve classification accuracy results above the 85% accuracy threshold in GLCW's (Becker, Lusch, & Qi, 2007; Becker, Lusch, & Qi, 2005). Using the ideal stretching method from the first research objective, bands were removed from a lidar-fused hyperspectral image based on their spectral distance (Table 3) from optimal bands identified by Becker et al. (2005).

Table 3.Distance from Optimal Band Centers and Order of Removal

Original Hyperspectral Band Centers (nanometers)	Distance to Closest Optimal Band	Closest Optimal Band	Order of Removal
1040.9	124.9	916	1
1019.5	103.5	916	2
998.1	82.1	916	3
976.7	60.7	916	4
632.5	52.5	685	5
611.0	51.0	560	6
374.5	50.5	425	7
869.3	46.7	916	8
955.2	39.2	916	9
847.8	35.8	812	10
460.4	35.4	425	11
481.9	32.1	514	12
654.1	30.9	685	13
761.7	30.7	731	14
589.5	29.5	560	15
395.9	29.1	425	16
783.3	28.7	812	17
890.8	25.2	916	18
933.8	17.8	916	19
826.3	14.3	812	20
438.9	13.9	425	21
546.4	13.6	560	22
718.7	12.3	731	23
697.1	12.1	685	24
524.9	10.9	514	25
503.4	10.6	514	26
675.6	9.4	685	27
740.2	9.2	731	28
568.0	8.0	560	29
417.4	7.6	425	30
804.8	7.2	812	31
912.3	3.7	916	32

The band with the greatest spectral distance from its closest optimal spectral band was removed first, and this process was continued until the lidar fused hyperspectral image was reduced to two bands, the minimum required for a classification routine. After each band was removed, neural network and maximum likelihood classification routines were performed and overall and cover type specific accuracies were compared to the classification accuracies of the original hyperspectral image. The overall and cover type specific classification accuracies for each spectrally reduced image were graphed to find the spectral resolution/band combination at

which overall and cover type specific classification accuracies begin to diminish or significantly change.

To test the final research objective, whether a synthetically derived aerial photography fused with ideally stretched lidar can achieve comparable overall and cover type specific classification accuracies to those classification accuracies achieved by original hyperspectral imagery, two classification accuracy assessments were performed. First, a synthetically derived aerial photograph fused with ideally stretched lidar was classified using both classification routines, and then assessed for its overall and cover type specific classification accuracy. Then the original hyperspectral image was classified using both classification routines, and also assessed for its overall and cover type specific classification accuracy. The two sets of classification accuracies were then compared to determine if synthetically derived aerial photography fused with ideally stretched lidar, which as a proxy for actual digital aerial photography fused with lidar, achieved accuracies comparable to those achieved by hyperspectral imagery.

CHAPTER IV

RESULTS

Objective One

Table 4 shows the resulting overall and average class accuracies of the hyperspectral and synthetically derived aerial photograph using both the neural network and the maximum likelihood classification routines for each stretching method. We found the neural network classifier produced the highest accuracy levels when using hyperspectral imagery without the integrated VHM band. However, when using the neural network classifier with synthetically derived aerial photography, applying a square root stretch to the integrated VHM band produced the highest overall and average producer's accuracies. When using a maximum likelihood classifier with hyperspectral imagery, it is most advantageous to apply a Gaussian stretch to the data, whereas applying no stretch to the integrated VHM band produced the highest overall and average producer's accuracies when using the SDAP imagery.

Table 4. Identified Ideal Stretching Methods.

	No Lidar	No Stretch	Linear	Equalize	Gaussian	Square Root
Overall Hyper NN	**94.97**	40.56	93.06	92.89	92.93	93.10
Class Avg Hyper NN	**87.41**	42.86	82.43	84.48	83.59	85.76
Overall Hyper ML	91.05	92.49	92.56	92.77	**92.74**	92.65
Class Avg Hyper ML	83.97	87.37	87.91	88.43	**88.52**	88.20
Overall SDAP NN	81.37	57.94	89.70	86.29	83.98	**91.06**
Class Avg SDAP NN	43.01	30.56	62.80	60.19	49.69	**64.84**
Overall SDAP ML	79.72	**84.23**	76.45	70.53	72.34	73.90
Class Avg SDAP ML	66.69	**77.28**	70.01	64.27	66.47	68.08

Objective Two

Overall, the integration of a VHM band into hyperspectral imagery helped to increase classification accuracies, using both maximum likelihood and neural network classification routines, until the seven spectral band threshold was reached, as shown by Figure 2.

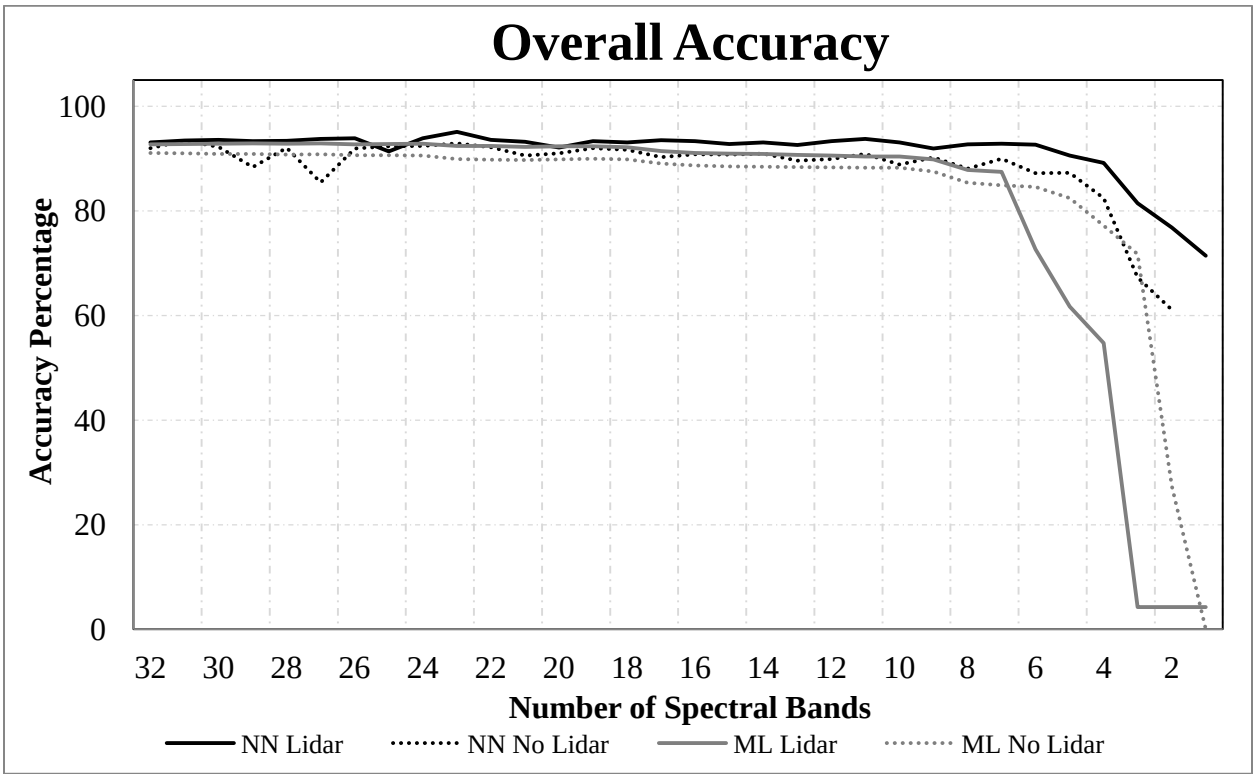

Figure 2. Overall Accuracies for Spectral Band Reduction Classifications

Once the number of spectral bands was reduced to less than seven, the accuracy results produced by the two classification routines behaved differently. The neural network classifier was able to maintain higher overall accuracies below the seven spectral bands threshold when using hyperspectral imagery fused with ideally stretched lidar, as opposed to using hyperspectral

imagery without lidar. Conversely, the maximum likelihood classifier achieved higher classification accuracies using hyperspectral imagery without a VHM band.

Due to the size and spectral dissimilarity of some of the cover types, overall accuracy does not accurately depict all of the results. The average producer's accuracy and the cover type specific producer's accuracy represent a more truthful portrayal of the classification accuracies. Figure 3 shows the average producer's accuracy for each band reduction classification.

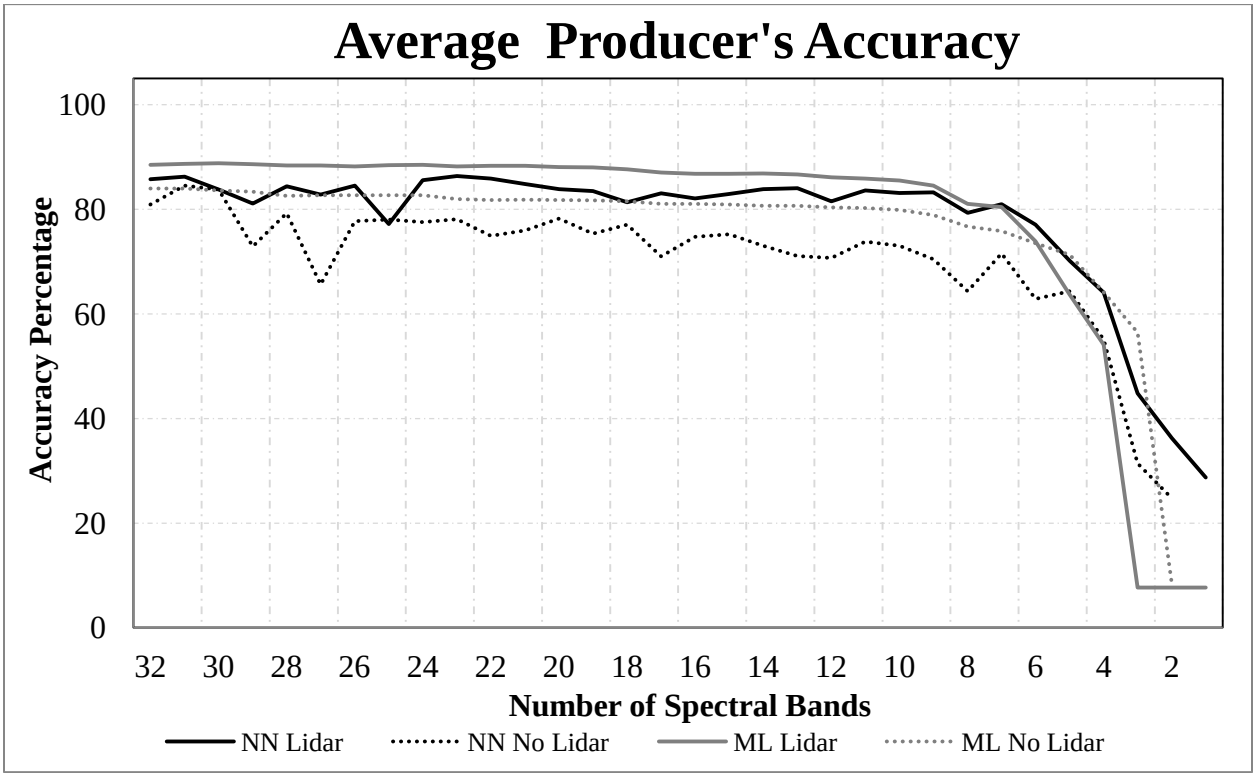

Figure 3. Average Producer's Accuracies for Spectral Band Reduction Classifications

The average producer's accuracy results shown in Figure 3 are similar to those shown by the overall accuracy results in Figure 2. One notable difference is the average producer's accuracy is slightly lower than the overall accuracy for all four classification routines, and once below the

seven spectral band threshold, the accuracy levels decrease more rapidly than do the corresponding overall accuracy results. Another important difference between overall accuracy and average producer's accuracy is the maximum likelihood classifier outperforms its neural network counterpart for hyperspectral imagery with and without the ideally stretched VHM band. Once the seven spectral bands threshold is reached, the neural network classification routine begins to achieve higher classification accuracy than its maximum likelihood counterparts. However, it should be noted that below the seven band threshold the average producer's accuracy falls below 80% for all classification routines.

To further understand what drives the difference between overall classification accuracy and average producers classification accuracy, select cover type specific producer's accuracies must be explained. First, for cover types with significant or/and homogeneous height components (i.e. Shrub, Tree, Willow), the integration of an ideally stretched VHM band allows both classification methods to more accurately identify a higher percentage of class member pixels, as opposed to the accuracies achieved by each classification routine on imagery without a lidar band. In these classes the maximum likelihood classification routine was more accurate and consistent when classifying both lidar and non-lidar fused imagery than the neural network classification routine.

The unique spectral signature of the Water class allowed both classification routines to achieve close to 100% classification accuracy until four spectral bands remained. With less than four spectral bands the height characteristics, or lack thereof, allowed the neural network classifier to maintain very high classification accuracy, even after the other classification routines began to fail.

The neural network and maximum likelihood classification routines were able to consistently achieve high producer's accuracies of the Submergent Vegetation cover type until the seven band threshold was reached. When using fewer than seven spectral bands, the maximum likelihood classification routine, both with and without ideally stretched lidar, was unable to differentiate between the similar spectral and/or height characteristics exhibited by the Submergent Vegetation and Broad Leaf Arrowhead cover types. The neural network classification routine, however, was able to maintain classification accuracies both with and without lidar below the seven spectral bands threshold. The Broad Leaf Arrowhead cover type was the least accurately classified cover type by all four classification routines. A likely reason for this could be the spectral signature/height component of this class is similar enough to the spectral signatures and height components exhibited by the other cover types that both classification routines are unable to consistently or accurately classify Broad Leaf Arrowhead.

The accuracies of the Bulrush cover type behaved similarly to those of the Broad Leaf Arrowhead cover type. The neural network classification routine was unable to consistently and accurately identify the Bulrush cover type, while the maximum likelihood classifier was able to correctly identify correct pixels, but lacked consistency. The reduced classification accuracy of the Bulrush cover type may likely be due to cross classification with the Shrub cover type. As spectral bands were reduced and more emphasis in the classifier is placed the VHM band, the confusion between the Bulrush and Shrub cover type most likely increased due to their similar height characteristics.

Wild Rice and Pickerelweed both lack a significant height characteristic because their sparseness/stem density does not allow the lidar data to derive a consistent height measurement. While both cover types have high producer's accuracies above the seven spectral bands

threshold, their classification accuracies significantly decreased with less than seven spectral bands. As meaningful spectral bands were removed, the lidar band caused confusion among classes with a non-influential lidar component as they played a more influential role in the classification routine.

The two vegetation cover types that dominate the study site, Cattails and Phragmites, are so dissimilar, both spectrally and with respect to height characteristics, that both cover types are accurately identified by both classification routines, with and without ideally stretched lidar, until the seven spectral bands threshold is reached. With less than seven spectral bands, the neural network classification routine is able to outperform the maximum likelihood classifier with and without the addition of lidar. Also, below the seven band threshold the integration of a VHM band allows the neural network classifier to maintain higher classification accuracy than when using imagery without the additional lidar band. The ability of the neural network classifier to utilize the lidar band to maintain high classification accuracies shows the importance of incorporating vegetation height characteristics, as derived from lidar data, into a spectral dataset for improvement in classification accuracies.

Objective Three

Figures 4 & 5 show the overall, average producer's, and cover type specific classification accuracies for the synthetically derived aerial photography without lidar, SDAP with lidar, and the hyperspectral image without lidar for the neural network (Figure 4) and maximum likelihood (Figure 5) classification methods. As Figure 4 shows, hyperspectral imagery, even without lidar, outperformed SDAP with and without ideally stretched lidar in the overall and class average categories, as well as most cover type specific categories when classified using a neural network.

However, it should be noted the addition of ideally stretched lidar to the SDAP image significantly improved overall and average producer's classification accuracies in comparison to the SDAP image without lidar. Three cover types in the SDAP with superiorly fused lidar, Spikerush, Tree, and Bulrush, outperform the hyperspectral imagery in regards to cover type specific classification accuracies.

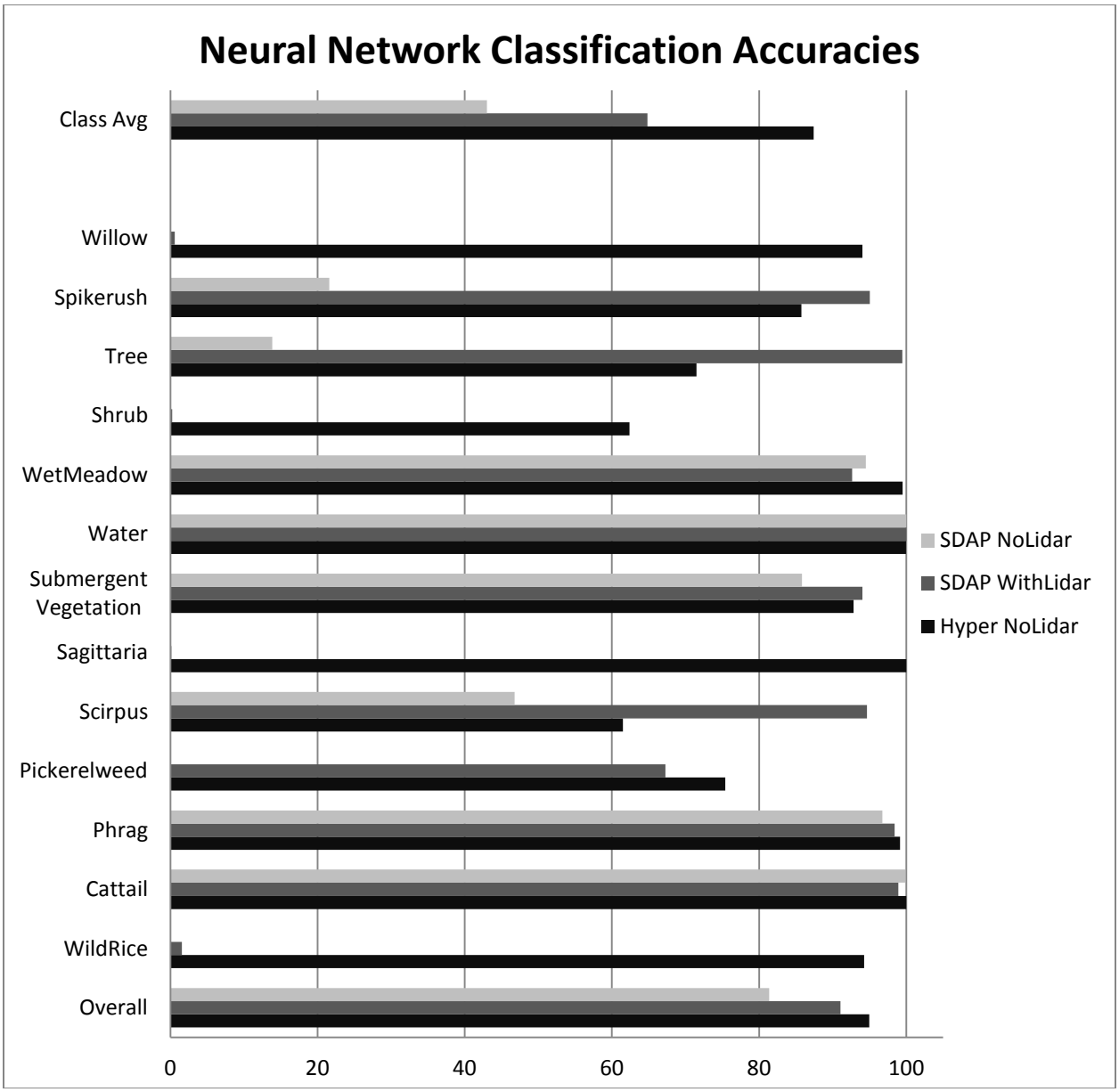

Fig. 4. Neural Network Classification Accuracies

The accuracy from the maximum likelihood classifications (Figure 5) shows results similar to the neural network classification accuracies in Figure 4. The hyperspectral imagery produced higher overall and average producer's classification accuracies, as well as performing better in most cover types. Again, it should be noted that the addition of ideally stretched lidar to

the SDAP increases classification accuracies, but not to the extent that is demonstrated in the neural network classification results. The maximum likelihood classified SDAP with ideally stretched lidar also has three cover types which outperform hyperspectral imagery classifications, but with maximum likelihood, the classes change to Spikerush, Shrub, and Broad Leaf Arrowhead.

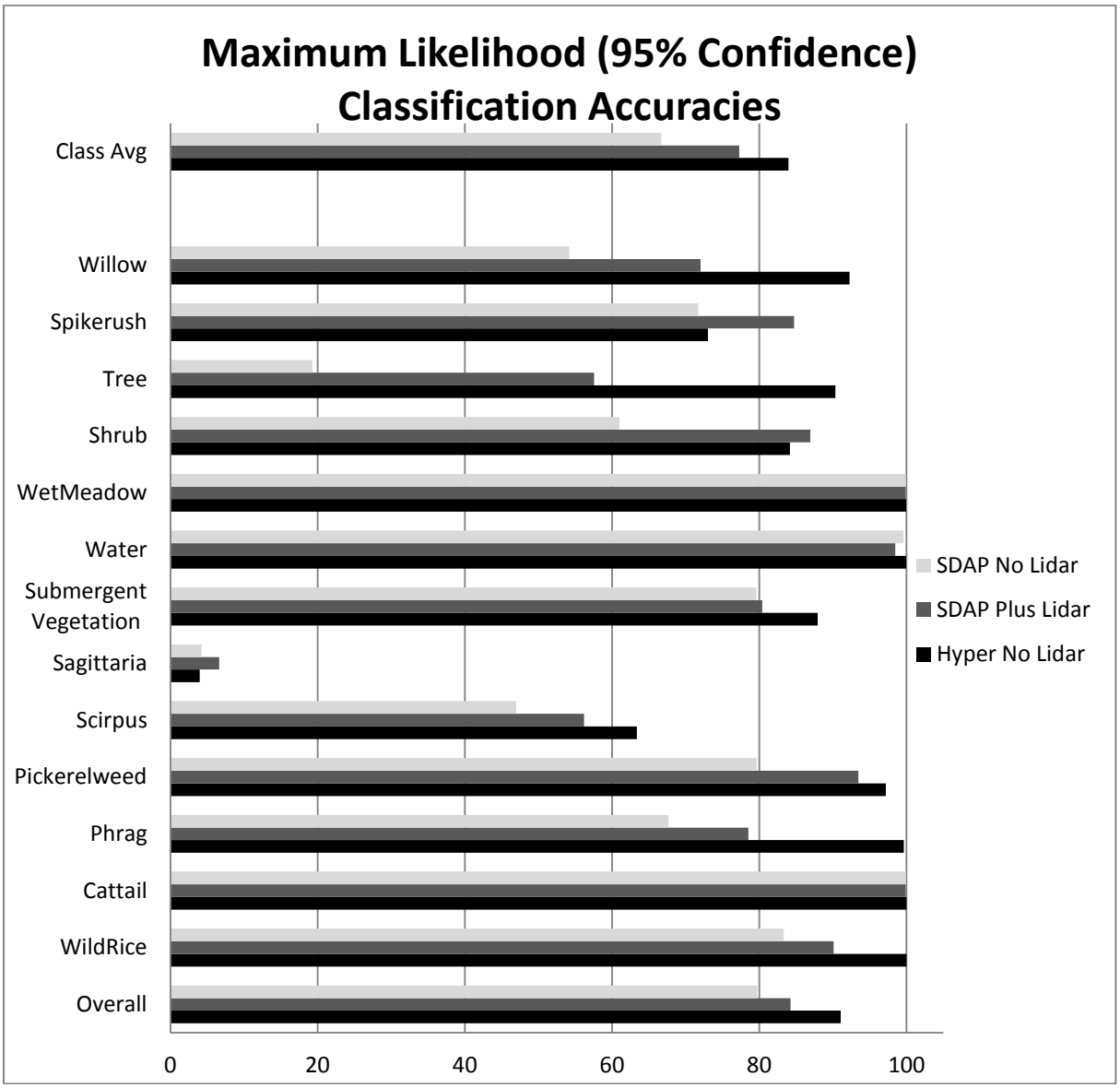

Fig. 5. Maximum Likelihood Classification Accuracies

CHAPTER V

CONCLUSIONS

The results from objective one show that when using a neural network classifier, it is most advantageous to apply a square root stretch to the lidar data before integrating it into the synthetically derived aerial photography. To explain this, the histogram of the square root stretched VHM band must be compared to the histogram of the of the other stretched VHM bands. The square root stretch is the stretching method that separates, or 'pulls apart' the histogram of the VHM band the most. This is advantageous when using the neural network classification because it creates the most randomness between connections within the classifier. With more apparently random training data, the neural network is better able to learn the training data, and assign more accurate network connection weights when determining class relationships within the neural network. That the neural network produces the highest accuracy results when using hyperspectral imagery without the addition of any lidar data could be attributed to the noise that the addition of a lidar band caused in the classification routine. Adding the lidar band to the hyperspectral imagery increases the amount of spectral data in the classification routine by approximately three percent. Since lidar data does not contain actual spectral reflectance data, but instead mimics it through stretching, its inclusion could be causing noise in the neural network therefore decreasing classification accuracies. The most advantageous stretching method for maximum likelihood classification can be explained primarily by the assumptions that this type of classification routine makes on the input dataset. Even though the ML classifier assumes the data to be normally distributed, the un-stretched VHM band is most advantageous to use with the synthetically derived aerial photograph. The most likely possibility for this is the reduced spectral dimensionality of the SDAP allows the un-stretched VHM band to dominate the

probability function used by the ML classifier by considerably separating the cover types in n-dimensional decision space. When classifying hyperspectral data fused with lidar using a maximum likelihood classification routine, it is most advantageous to apply a Gaussian stretch to the VHM band. This can be simply explained by the statistical assumptions, as mentioned above, that the maximum likelihood classification routine makes on input data.

While not every class can be specifically explained through its height characteristics as described by the VHM band, the inclusion of this data did result in an increase in some cover type specific classification accuracies, as well as an increase in overall classification accuracies when included with hyperspectral imagery. This is consistent with the findings of Dalponte et al. (2008), and Mundt et al. (2006), who both showed that the inclusion of lidar derived data in a classification routine can increase overall and some cover type classification accuracies. In concurrence with Becker et. al (2005), we found that when incorporating lidar data into hyperspectral imagery there still needs to be a minimum of seven strategically placed spectral bands in order to achieve high classification accuracies. We found even with the inclusion of ideally stretched lidar, spectral seperability can only be achieved with the seven band placements demonstrated by Becker et al. (2005). The information provided by the VHM band is not able to take the place of one of the seven spectral bands; instead, it provides increased classification accuracy for the number of spectral bands included in the classification routine.

The addition of an ideally stretched lidar band to a synthetically derived aerial photograph was able to increase overall and average producer's classification accuracies when compared to classification results of SDAP without ideally stretched lidar data. The ability of a ideally stretched lidar band fused with SDAP to increase classification accuracies was demonstrated by both the neural network and the maximum likelihood classification routines.

This increase in classification accuracies is a direct result of the additional 'spectral' information (i.e. lidar data) included in the classification routine. If you think about the VHM band as an additional spectral band, where the plant height values are substitutes for percent reflectance values, the inclusion of the VHM band increases the spectral dimensionality of the image by 20%. However, the addition of the VHM band to the synthetically derived aerial photograph did not allow it to achieve classification accuracies that are comparable to those achieved by hyperspectral imagery. While the VHM band did increase the spectral dimensionality of the SDAP, it did not come close to matching the spectral dimensionality of the hyperspectral image. This further showed that at least seven strategically placed spectral bands are necessary to achieve high classification accuracies. Furthermore, the increase in classification accuracies helped to show that the utilization of lidar data is beneficial when classifying imagery with lower spectral resolution.

The increase in classification accuracies for a given number of spectral bands showed the VHM band and the multi/hyperspectral dataset to contain complementary information, and when used together in a classification routine, they can provide a more detailed classification result. The inclusion of lidar has been shown to be most beneficial, in regards to its ability to increase classification accuracies, when using a spectrally reduced dataset (i.e. synthetically derived aerial photography, or its real world equivalent, digital aerial photography). However, for the integration of lidar to be truly beneficial, its collection and acquisition must be cost effective. To accomplish this, both datasets should be collected in close temporal proximity, preferably during the same flight. Then to accurately include the lidar data in a classification routine, it must be co-registered with its corresponding imagery. Finally, the lidar data should be ideally stretched before being fused with the imagery that will also be included in the classification routine.

REFERENCES

Anderson, J. E., Plourde, L. C., Martin, M. E., Braswell, B. H., Smith, M.-L., Dubayah, R. O., . . . Blair, J. B. (2008). Integrating Waveform LIDAR with Hyperspectral Imagery for Inventory of a Northern Temperate Forest. *Remote Sensing of Environment, 112*, 1856-1870.

Atkinson, P. M., & Tatnall, A. R. (1997). Neural Networks in Remote Sensing. *International Journal of Remote Sensing, 18*(4), 699-709.

Axelsson, P. (1999). Procssing of Laser Scanner Data-Algorithms and Applications. *ISPRS Journal of Photogrammetry & Remote Sensing, 54*, 138-147.

Becker, B. L. (2002). *A Classification-Based Assessment of the Optimal Spatial and Spectral Resolution of Coastal Wetland Imagery.* Michigan State University.

Becker, B. L., Lusch, D. P., & Qi, J. (2005). Identifying Optimal Spectral Bands From In-Situ Measurements of Great Lakes Coastal Wetlands Using Second-Derivative Analysis. *Remote Sensing of Environment, 97*(2), 238-248.

Becker, B. L., Lusch, D. P., & Qi, J. (2007). A Classsification-Based Assessment of the Optimal Spectral and Spatial Resolutions for Great Lakes Coastal Wetland Imagery. *Remote Sensing of Environment, 108*(1), 111-120.

Bork, E. W., & Su, J. G. (2007). Integrating LIDAR Data and Multispectral Imagery for Enhanced Classification of Rangeland Vegetation: A Meta Analysis. *Remote Sensing of Environment, 111*, 11-24.

Brennan, R., & Webster, T. L. (2006). Object-Oriented Land Cover lassificaiton of LIDAR-Derived Surfaces. *Canadian Journal of Remote Sensing*, 162-172.

Dalponte, M., Bruzzone, L., & Gianelle, D. (2008). Fusion of Hyperspectral and LIDAR Remote Sensing Data for Classification of Complex Forest Areas. *IEEE Transactions on Geoscience and Remote Sensing, 46*(5), 1416-1427.

Galvao, L. S., Formaggio, A. R., & Tisot, D. A. (2005). Discrimination of Sugarcane Varieties in Southeastern Brazil with EO-1 Hyperion Data. *Remote Sensing of Environment, 94*, 523-534.

Gilmore, M. S., Wilson, E. H., Barrett, N., Civco, D. L., Prisloe, S., Hurd, J. D., & Chadwick, C. (2008). Integrating Multi-temporal Spectral and Structural Information to Map Wetland Vegetation in a Lower Connecticut River Tidal Marsh. *Remote Sensing of Environment, 112*, 4048-4060.

Govender, M., Chetty, K., Naiken, V., & Bulcock, H. (2008). A Comparison of Satellite Hyperspectral and Multispectral Remote Sensing Imagery for Improved Classification and Mapping of Vegetation . *Water SA, 34*(2), 147-154.

Haskett, H. T., & Sood, A. K. (1998, April). Trade-off Studies of Detection Performance Versus the Number of Reflective Spectral Bands in Hyperspectral Imagery. *SPIE Conference on Algorithms for Multispectral and Hyperspectral Imagery IV, 3372*, pp. 26-42. Orlando, Flordia.

Hyde, P., Ross, N., Kimes, D., & Levine, E. (2007). Exploring LiDAR–RaDAR Synergy—Predicting Aboveground Biomass in a Southwestern Ponderosa Pine Forest Using LiDAR, SAR and InSAR. *Remote Sensing of Environment, 106*(1), 28-38.

Jones, T. G., Coops, N. C., & Sharma, T. (2010). Assessing the Utility of Airborne Hyperspectral and LiDAR Data for Species Distribution Mapping in the Coastal Pacific Northwest, Canada. *Remote Sensing of Environment, 114*, 2841-2852.

Key, T., Warner, T. A., McGraw, J. B., & Fajvan, M. A. (2001). A Comparison of Multispectral and Multitemporal Information in High Spatial Resolution Imagery for Classification of Individual Tree Species in a Temperate Hardwood Forest. *Remote Sensing of Environment, 75*(1), 100-112.

Koonce, J. F., Minns, C. K., & Morrison, H. A. (1998). Biodiversity Investment Areas, Aquatic Ecosystems. *State of the Lakes Ecosystem Confrence* .

Kraus, K., & Pfeifer, N. (1998). Determination of Terrain Models in Wooded Areas with Airborne Laser Scanner Data. *ISPRS Journal of Photogrammetry and Remote Sensing, 53*, 193-203.

Kumar, U., & Ramachandra, T. V. (2008). Endmembers Discrimination in MODIS Using Spectral Angle Mapper and Maximum Likelihood Algorithms. *International Journal of Applied Remote Sensing, 2*(1), 1-14.

Maas, H.-G. (1999, June 21-24). The Potential of Height Texture Measures for the Segmentation of Airborne Laserscanner Data. *4th International Airborne Remote Sensing Conference and Exhibition and 21st Canadian Symposium on Remote Sensing.* Ottawa, Ontario, Canada.

Maynard, L., & Wilcox, D. (1997). Coastal Wetlands of the Great Lakes, background paper for the State of the Lakes Ecosystem Conference 1996.

Mundt, J., Streutker, D., & Glenn, N. (2006). Mapping Sagebrush Distribution Using Fusion of Hyperspectral and LIDAR Classifications. *Photogrammetric Engineering and Remote Sensing, 72*(1), 47-54.

Onojeghuo, A. O., & Blackburn, G. A. (2011). Optimising the Use of Hyperspectral and LiDAR Data for Mapping Reedbed Habitats. *Remote Sensing of Environment, 115*, 2025-2034.

Plourde, L. C., Ollinger, S. V., Smith, M.-L., & Martin, M. E. (2007). Estimating Species Abundance in a Northern Temperate Forest Using Spectral Mixture Analysis. *Photogrammetric Engineering and Remote Sensing, 73*(7), 829-840.

Reed, B. C., Brown, J. F., VanderZee, D., Loveland, T. R., Merchand, J. W., & Ohlen, D. O. (1994). Measuring Phenological variability from Satellite Imagery. *Journal of Vegetation Science, 5*(5), 703-714.

Shafri, H. Z., Suhaili, A., & Mansor, S. (2007). The Performance of Maximum Likelihood, Spectral Angle Mapper, Neural Network and Decision Tree Classifies in Hyperspectral Image Analysis. *Journal of Computer Science, 3*(6), 419-423.

Simental, E., Dubayah, R., Walker, W., Blair, J. B., Hofton, M., & Hunsaker, C. (2006). Mapping Forest Structure for Wildlife Habitat Analysis Using Multi-Sensor (LiDAR, SAR/InSAR, ETM+, Quickbird) Synergy. *Remote Sensing of Environment, 102*, 63-73.

Simental, E., Ragsdale, D., Bosch, E., Dodge, J. R., & Pazak, R. (2003, May 3-9). Hyperspectral Dimension Reduction and Elevation Data for Supervised Image Classification. *Proc. 14th ASPRS Conf.* .

Underwood, E., Ustin, S., & Dipietro, D. (2003). Mapping Non-Native Plants Using Hyperspectral Imagery. *Remote Sensing of Environment, 86*(2), 150-161.

Vosselman, G. (2000). Slope Based Filtering of Laser Altimetry Data. *International Archives of Photogrammetry and Remote Sensing, 33*, 935-942.

Williams, A. P., & Hunt Jr., E. R. (2002). Estimation of Leafy Spurge Cover from Hyperspectral Imagery Using Mixture Tuned Matched Filtering. *Remote Sensing of Environment, 82*(2-3), 446-456.

Yamano, H., Chen, J., & Tamura, M. (2003). Hyperspectral Identification of Grassland Vegetation in Xilinhot, Inner Mongolia, China. *International Journal of Remote Sensing, 24*(15), 3171-3178.

Zhang, K., Chen, S.-C., Whitman, D., Shyu, M.-L., Yan, J., & Zhang, C. (2003). A Progressive Morphological Filter for Removing Nonground Measurements From Airborne LIDAR Data. *IEEE Transactions on Geoscience and Remote Sensing, 41*(4), 872-882.